Journal of Power Sources 187 (2009) 348–355

Contents lists available at ScienceDirect

Journal of Power Sources

journal homepage: www.elsevier.com/locate/jpowsour

Characterization of Cu, Ag and Pt added $La_{0.6}Sr_{0.4}Co_{0.2}Fe_{0.8}O_{3-\delta}$ and gadolinia-doped ceria as solid oxide fuel cell electrodes by temperature-programmed techniques

Ta-Jen Huang*, Xian-De Shen, Chien-Liang Chou

Department of Chemical Engineering, National Tsing Hua University, Hsinchu 30013, Taiwan, ROC

ARTICLE INFO

Article history:
Received 23 September 2008
Received in revised form 28 October 2008
Accepted 5 November 2008
Available online 17 November 2008

Keywords:
Temperature-programmed oxidation
Temperature-programmed reduction
Characterization
Cathode
Anode
Solid oxide fuel cell

ABSTRACT

Cu, Ag and Pt added $La_{0.6}Sr_{0.4}Co_{0.2}Fe_{0.8}O_{3-\delta}$ (LSCF) and gadolinia-doped ceria (GDC) were analyzed by the temperature-programmed techniques for their characteristics as either the cathode or the anode of the solid oxide fuel cells (SOFCs). Temperature-programmed oxidation using CO_2 was used to characterize the cathode materials while temperature-programmed reduction (TPR) using H_2 and TPR using CO were used to characterize the anode materials. These techniques can offer an easy screening of the materials as the SOFC electrodes. The effects of adding Cu, Ag and Pt to LSCF for the cathodic reduction activity and the anodic oxidation activity are different—Cu > Ag > Pt for reduction and Pt > Cu > Ag for oxidation. The CO oxidation activities are higher than the H_2 oxidation activities. Adding GDC to LSCF can increase both reduction and oxidation activities. The LSCF–GDC composite has a maximum activity for either reduction or oxidation when LSCF/GDC is 2 in weight.

1. Introduction

The $La_{1-x}Sr_xCo_{1-y}Fe_yO_{3-\delta}$ (LSCF) perovskites have been considered as the cathode materials for the solid oxide fuel cells (SOFCs) to replace the conventional $La_{1-x}Sr_xMnO_{3-\delta}$ (LSM) materials [1–4]. This is attributed to the high catalytic activity of LSCF for oxygen reduction. The oxygen reduction activity of LSCF can be one order of magnitude higher than that of LSM [5], especially of the A-site deficient $La_{0.58}Sr_{0.4}Co_{0.2}Fe_{0.8}O_{3-\delta}$ perovskite [6]. This is an important characteristic for SOFCs when the operating temperature is reduced. However, as the operating temperature of an SOFC is decreasing, a higher activity of oxygen reduction becomes increasingly important and thus the adding of metals into the cathode material to increase its oxygen reduction activity has been the subject of numerous studies; the metals which have been studied include Pt [7–10], Pd [11], Ag [9,12–14] and Cu [15–17]. Copper has also been studied as a component in the perovskite materials as the SOFC cathodes [18,19].

The LSCF perovskites have also been considered as the SOFC anode materials [20]. Other La and Sr based perovskites have also been studied as the SOFC anode materials so as to have an enhanced anodic activity [21,22]. The anodic activity can also be enhanced with the addition of metals, such as Pt [23] and Cu [24]; these metals are used especially for suppressing coking, which is a serious problem during direct oxidation of methane in SOFCs [25]. Nevertheless, Ag is seldom used in the SOFC anode materials.

Gadolinia-doped ceria (GDC) is the well-known materials in the SOFC anodes [26]. The mixing of GDC with LSCF to form the LSCF–GDC composite has been shown to increase the adhesion of the cathode materials to the YSZ electrolyte [27]. With LSCF being $La_{0.6}Sr_{0.4}Co_{0.2}Fe_{0.8}O_{3-\delta}$ and GDC being $Ce_{0.8}Gd_{0.2}O_{2-\delta}$, the LSCF–GDC composite can perform better than pure LSCF as the SOFC cathode [10]. The addition of 50 vol.% GDC to LSCF has resulted in a decrease of the polarization resistance with a factor of about 10 compared to that of the LSCF cathode [28]. On the other hand, LSCF–GDC has also been used as anode materials for the direct oxidation of methane in intermediate-temperature SOFCs and shown to have no formation of carbon deposits [29].

The characterization of the SOFC cathode materials is frequently performed by the impedance spectroscopic measurements [5,10,28]. This impedance spectroscopic result is usually quite complex, since there coexist many resistances, such as the resistance for the oxygen exchange reaction at the electrode surface, the oxygen–ion transfer resistance at the electrode/electrolyte interface, and the oxygen–ion conducting resistance in the electrolyte [30]. Thus, the impedance result may not be directly related to the oxygen reduction activity of the cathode materials.

* Corresponding author. Tel.: +886 3 5716260; fax: +886 3 5715408.
E-mail address: tjhuang@che.nthu.edu.tw (T.-J. Huang).

0378-7753/$ – see front matter © 2008 Elsevier B.V. All rights reserved.
doi:10.1016/j.jpowsour.2008.11.019

A measurement of temperature-programmed oxidation using carbon dioxide (CO_2-TPO) [31] may be applicable to analyze the characteristics of the SOFC cathode materials. This can be a relatively direct analysis of the SOFC cathode characteristics since the reaction of CO_2-TPO is the dissociative adsorption of CO_2, $CO_2 \rightarrow CO + O$, and the produced O species can fill into the surface oxygen vacancy or transport into the oxygen vacancy in the bulk lattice [32,33]. Since the oxygen reduction mechanism consists of oxygen adsorption, charge transfer reaction and oxygen incorporation into the oxygen vacancy [17], the oxygen reduction activity may be analyzed by the CO_2-TPO measurements.

In this work, Cu, Ag and Pt added LSCF and GDC as well as various LSCF–GDC composites, all in the powder forms, were analyzed by CO_2-TPO for their characteristics as the SOFC cathodes. Current–voltage and AC impedance measurements in SOFC unit cells were performed to confirm the feasibility of the CO_2-TPO characterization for the cathode materials. These materials were also analyzed by temperature-programmed reduction (TPR) using H_2 and TPR using CO for their characteristics as the SOFC anodes. It was shown that these temperature-programmed techniques can offer an easy screening of the materials as the SOFC electrodes.

2. Experimental

2.1. Preparation of LSCF and GDC and metal addition

LSCF was prepared by the glycine–nitrate process with a composition of $La_{0.6}Sr_{0.4}Co_{0.2}Fe_{0.8}O_{3-\delta}$. The A-site deficient LSCF was also prepared and its composition was $La_{0.58}Sr_{0.4}Co_{0.2}Fe_{0.8}O_{3-\delta}$, denoted as L58SCF. Appropriate amounts of reagent-grade (Showa, Japan) metal nitrates $La(NO_3)_3{\cdot}6H_2O$, $Sr(NO_3)_2$, $Co(NO_3)_2{\cdot}6H_2O$ and $Fe(NO_3)_3{\cdot}9H_2O$ were dissolved in de-ionized water. Glycine (Sigma, USA) was also dissolved in de-ionized water. Then, these two solutions were mixed together with a glycine to NO_3 ratio of 1:0.8. The mixture was then heated under stirring at 110 °C until combustion occurred. The obtained product was ground to powders. The LSCF powders were calcined by heating in air at a rate of 5 °C min^{-1} to 500 °C and held for 2 h, then to 900 °C and held for 4 h, and then slowly cooled down to room temperature.

GDC was prepared by the co-precipitation method with a composition of $Ce_{0.8}Gd_{0.2}O_{2-\delta}$. The details of the method have been described elsewhere [34]. The GDC powders were calcined by heating in air at a rate of 5 °C min^{-1} to 900 °C and held for 4 h before cooling down.

The LSCF–GDC composite was prepared by mixing the above-prepared LSCF and GDC powders. The mixture was ground for 24 h and then calcined by heating in air at a rate of 5 °C min^{-1} to 500 °C and held for 2 h, and then to 900 °C and held for 10 h before cooling down.

The metal addition to L58SCF, LSCF, GDC and LSCF–GDC powders was done by impregnation. The Cu, Ag and Pt cation solutions were prepared by dissolving $Cu(NO_3)_2{\cdot}3H_2O$ (Showa, Japan), $AgNO_3$ (Hwang Long, Taiwan) and $H_2Pt(OH)_6$ (Aldrich, USA) in de-ionized water, respectively. After drying, the powders were calcined by heating in air at a rate of 5 °C min^{-1} to 900 °C and held for 4 h before cooling down. The metal loading in this work was always 2 wt.% in terms of the weight of LSCF in metal-added LSCF or LSCF–GDC or the weight of GDC in metal-added GDC.

2.2. Current–voltage and AC impedance measurements in SOFC unit cell

The commercial YSZ tape (Jiuhow, Taiwan) was employed to make an electrolyte-supported SOFC cell. A disk of 1.8 cm in diameter was cut from the tape. One side of the disk was spin-coated with the paste of Ni-GDC as the anode, being composed of 60 wt.% Ni in terms of GDC, which has been shown to have an optimum anode performance [25]. The details of the preparation of the Ni-GDC paste have been described elsewhere [35]. The other side of the disk was spin-coated with a thin LSCF–GDC interlayer to enhance adhesion and then with L58SCF or metal-added L58SCF as the cathode. The thus-prepared SOFC unit cell has an anode-layer thickness of 25 μm, an electrolyte-layer thickness of 156 μm, an interlayer thickness of 5 μm, a cathode-layer thickness of 20 μm, and a cathode area of 1.1 cm^2.

The measurement of current–voltage (I–V) curve was performed at 800 °C with pure hydrogen on the anode side and 20% O_2 in Ar on the cathode side, both at a flow rate of 100 ml min^{-1}. The voltage was varied by an adjustable resister, and both the voltage and the current were measured by a Multimeter (TES 2730). The AC impedance measurement was done by an Electrochemical Analyzer (CHI608A, CH Instruments, USA) with a scanning frequency range of 1 MHz to 0.01 Hz and an amplitude of 50 mV. The working electrode was connected to the anode current collector, and both the reference electrode and the counter electrode were connected to the cathode current collector. The AC impedance measurements were performed under the same operating conditions as those of I–V curves.

2.3. CO_2-TPO measurement

The CO_2-TPO measurement was conducted under atmospheric pressure in a continuous flow reactor charged with 25 mg of sample powders. Some details of the CO_2-TPO measurement have been described elsewhere [31].

The powders were dried in the reactor, and then reduced by heating at a rate of 10 °C min^{-1} in 30 ml min^{-1} of 10% H_2 in Ar to 900 °C and then held at 900 °C for 30 min. Then, the powders were cooled down to room temperature in argon flow. Then, CO_2-TPO was performed with 30 ml min^{-1} of 10% CO_2 in Ar from room temperature to 900 °C at a rate of 10 °C min^{-1} and then held at 900 °C for 30 min before cooling down. The reactor outflow was analyzed on-line by a CO-NDIR (non-dispersive infrared analyzer, Beckman 880).

2.4. Temperature-programmed reduction using H_2 or CO

Temperature-programmed reduction using hydrogen (H_2-TPR) and temperature-programmed reduction using carbon monoxide (CO-TPR) were performed at atmospheric pressure in a continuous flow reactor charged with 25 mg of sample powders. H_2-TPR tests

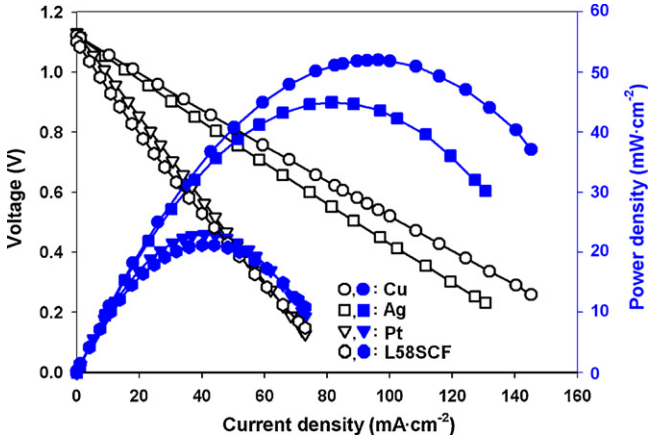

Fig. 1. Current–voltage and power density profiles of L58SCF and Cu, Ag and Pt added L58SCF as SOFC cathodes.

Table 1
Maximum power density and AC impedance over Cu, Ag and Pt added L58SCF as SOFC cathodes.

Cathode materials	Maximum power density ($mW\,cm^{-2}$)	AC impedance[a] ($\Omega\,cm^2$)
Cu-L58SCF	51.8	1.22
Ag-L58SCF	45	1.9
Pt-L58SCF	23	3.41
L58SCF	21.3	3.86

[a] The impedance value was determined by the overall width of the arcs.

were performed with 10% H_2 in Ar at a flow rate of $30\,ml\,min^{-1}$, heated from room temperature to 900 °C at a rate of $10\,°C\,min^{-1}$ and then held at 900 °C for 30 min. Some details of the H_2-TPR test have been presented elsewhere [36].

CO-TPR tests were performed using the same temperature program as that of H_2-TPR but with $30\,ml\,min^{-1}$ of 10% CO in Ar. The powders were calcined at 900 °C with $30\,ml\,min^{-1}$ of 20% O_2 in Ar for 1 h and then cooled down in argon flow to room temperature before carrying out the CO-TPR test. During CO-TPR, the reactor outflow was analyzed on-line by a CO_2-NDIR (Beckman 880).

After CO-TPR and held at 900 °C, the reactor was purged with argon flow for 30 min. Then, possible residual carbon over the powders was removed with $30\,ml\,min^{-1}$ of 20% O_2 in Ar at 900 °C. The reactor outflow was analyzed on-line by both CO-NDIR and CO_2-NDIR.

3. Results

3.1. Performance of current–voltage and AC impedance

Fig. 1 presents the current–voltage and power density profiles of the SOFC unit cells with cathodes made of L58SCF, $La_{0.58}Sr_{0.4}Co_{0.2}Fe_{0.8}O_{3-\delta}$, an A-site deficient LSCF, and Cu, Ag and Pt added L58SCF. These SOFC unit cells were the same except the cathode materials. The resulted maximum power density is listed in Table 1. The addition of the metals all increases the maximum power density over that of pure L58SCF cathode. The effect of metal addition on the maximum power density has a trend Cu > Ag > Pt. However, there is no difference in the current–voltage performance at open circuit, i.e., zero current density, which is the operating condition for the AC impedance measurement.

Fig. 2 shows the AC impedance spectra with the resulting overall impedances presented in Table 1. Due to the complexity in the interpretation of the impedance results, this work reports only the observed overall impedance that is the impedance as determined by the overall width of the arcs. The addition of the metals all decreases the impedance in comparison to that of pure L58SCF cathode. The effect of metal addition on the impedance has a trend Cu < Ag < Pt; this agrees with the trend of maximum power density since smaller impedance leads to larger electrochemical reaction rate, resulting in larger maximum power density. Notably, the impedance spectra show an indirect SOFC performance while the power density from the *I–V* measurement shows a relatively direct SOFC performance.

3.2. CO_2-TPO analysis for cathode characterization

The SOFC cathode needs an activity for O_2 reduction, which is to take in the O species from the cathode-side gaseous oxygen and to incorporate it into the oxygen vacancy in the lattice of the oxygen–ion conducting cathode materials. The O_2 reduction consists of O_2 dissociation to produce the O species and the transport of the O species into the lattice [17]. When the step of dissociation to produce the O species is not rate determining, which is possibly the case at high temperature, the interfacial transport of the oxygen species from the surface to the oxygen vacancy in the lattice becomes important, which is

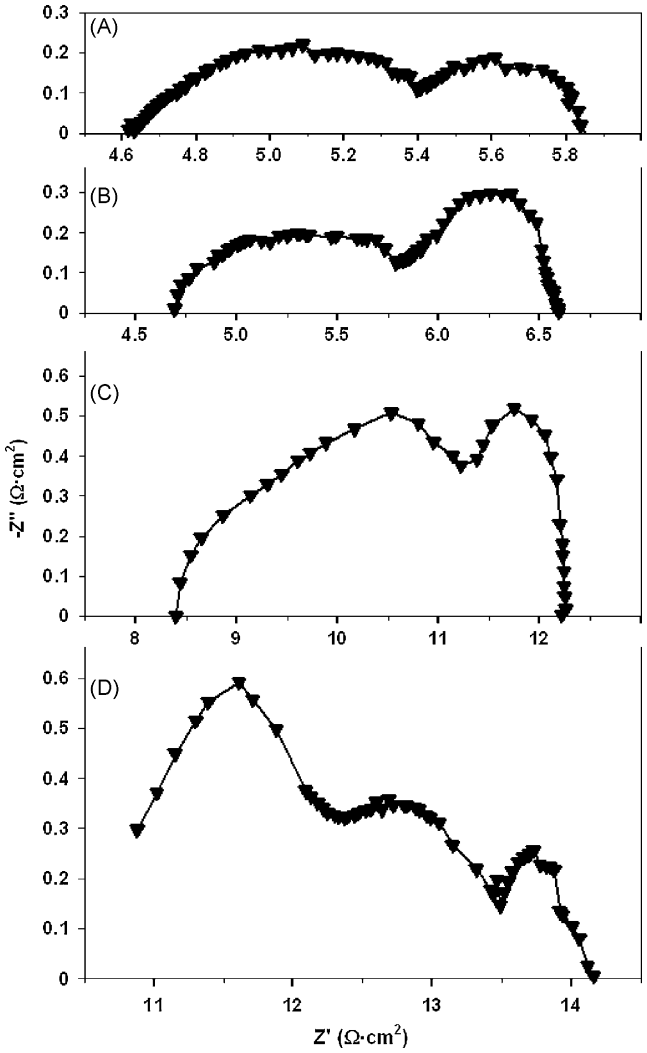

Fig. 2. AC impedance spectra of L58SCF and Cu, Ag and Pt added L58SCF as SOFC cathodes: (A) Cu-L58SCF, (B) Ag-L58SCF, (C) L58SCF, (D) Pt-L58SCF.

$$O_{surface} \leftrightarrows O_{lattice} \quad (1)$$

In this case, the O_2 reduction activity can be equal to the activity of CO_2 reduction, which consists of the following step of CO_2 dissociation to produce the O species

$$CO_2 \rightarrow CO + O \quad (2)$$

where O is the surface O species, which should be transported into the oxygen vacancy in the lattice to complete the process of CO_2 reduction. This indicates a similarity between the process of electrochemistry, which includes ion and electron transfers, over SOFC cathode and the process of chemistry in the CO_2-TPO analysis—that is, both have reaction (1) as the rate-determining step. Notably, the rate of either ion or electron transfer is not rate determining. Therefore, the CO_2-TPO analysis may be feasible to characterize the materials as the SOFC cathode. As O_2 reduction is sometimes referred as O_2 dissociation, CO_2 reduction is referred as CO_2 dissociation in this work.

Fig. 3 shows CO_2-TPO profiles of L58SCF and Cu, Ag and Pt added L58SCF, while Table 2 lists the resulted overall peak area in terms of the total amount of CO formation. Notably, a larger amount of CO formation represents a larger activity of CO_2 disso-

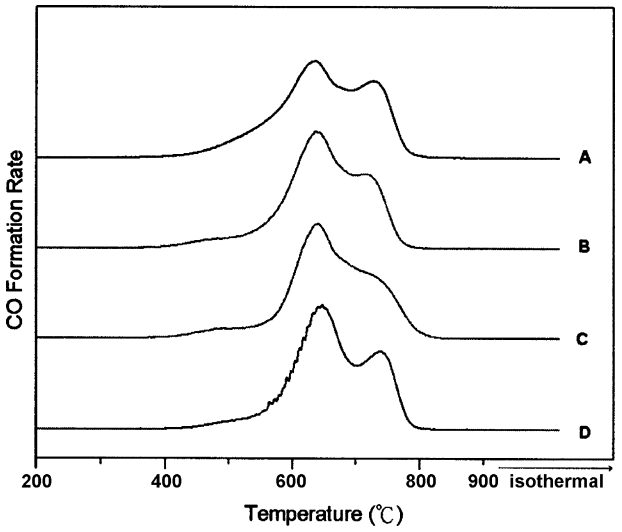

Fig. 3. CO_2-TPO profiles: (A) Cu-L58SCF, (B) Ag-L58SCF, (C) Pt-L58SCF, (D) L58SCF.

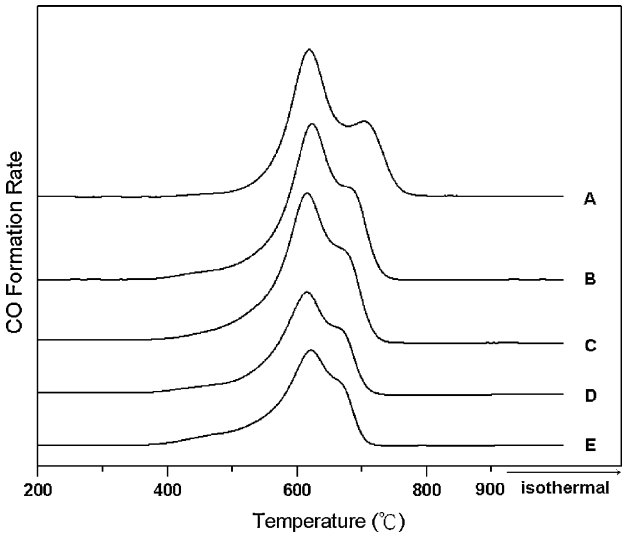

Fig. 4. CO_2-TPO profiles: (A) LSCF, (B) 100LSCF–30GDC, (C) 100LSCF–50GDC, (D) 100LSCF–70GDC, (E) 100LSCF–100GDC.

ciation [31]; thus, the CO_2-TPO activity represents the activity of CO_2 dissociation. The CO_2-TPO activity shows a trend Cu > Ag > Pt, which is the same as that of the SOFC performances in terms of both current–voltage and AC impedance with Cu, Ag and Pt added L58SCF as cathodes. This confirms the feasibility of the CO_2-TPO characterization for the cathode materials. Therefore, the CO_2-TPO analysis can be employed for screening the materials as the SOFC cathode.

Since L58SCF has been shown to have a better SOFC performance than that of LSCF as cathode [37], a comparison of the CO_2-TPO activity of L58SCF with that of LSCF is performed in this work; the CO_2-TPO results are shown in Table 2. The CO_2 reduction activity, in terms of the total amount of CO formation during CO_2-TPO, over L58SCF is larger than that over LSCF; this is in agreement with a comparison of SOFC performance in terms of the current density [37]. Additionally, over Cu, Ag and Pt added L58SCF, the CO_2-TPO activity is larger than that over Cu, Ag and Pt added LSCF, respectively, and the activities also show a trend Cu > Ag > Pt. Notably, the CO_2 reduction activity is represented by the CO_2-TPO activity. Therefore, the trend in CO_2 reduction activities can represent that in O_2 reduction activities.

3.3. Temperature-programmed analyses of various LSCF–GDC composites

Murray et al. [28] reported that the LSCF–GDC composite with 50 vol.% GDC has a much lower polarization resistance than LSCF as the SOFC cathodes. The LSCF–GDC composite has also been used as the anode for direct oxidation of methane in intermediate-temperature SOFCs [29]. Therefore, the LSCF–GDC composites with various compositions were analyzed in this work by the temperature-programmed techniques to characterize their activities not only as the SOFC cathode but also as the SOFC anode.

Fig. 4 shows the CO_2-TPO profiles of various LSCF–GDC composites, while Table 3 lists the resulted overall peak area in terms of the total amount of CO formation. With LSCF/GDC being 2 in weight, 100LSCF–50GDC has the highest CO_2-TPO activity among these composites and its activity is higher than that of LSCF. This indicates a synergistic effect since the CO_2-TPO activity of GDC is almost negligible. With GDC content larger than that in 100LSCF–50GDC, the CO_2-TPO activity of the LSCF–GDC composite becomes smaller than that of LSCF, as shown in Table 3.

The total amounts of CO formation during CO_2-TPO over Cu, Ag and Pt added 100LSCF–50GDC are presented in Table 2. Metal additions all enhance the CO_2-TPO activity. The CO_2-TPO activities show a trend Cu > Ag > Pt, which is the same as that of metal-added LSCF. However, Table 2 also reveals that the CO_2-TPO activities of Cu, Ag and Pt added GDC show a trend Pt > Ag > Cu, which is a reverse to that of metal-added LSCF. Nevertheless, the CO_2-TPO activity of even the Pt-added GDC is much smaller than that of LSCF; this renders GDC to be not applicable to utilization as the SOFC cathode.

Table 3 also shows the total amounts of H_2 consumption during H_2-TPR and those of CO_2 formation during CO-TPR over various LSCF–GDC composites. Notably, both H_2-TPR and CO-TPR are for the characterization of the materials as the SOFC anode; the H_2-TPR activity represents the activity of H_2 oxidation to form H_2O and the CO-TPR activity represents the activity of CO oxidation to form CO_2. Either H_2-TPR or CO-TPR needs to extract oxygen species from the lattice and to transport it to the surface for oxidation, a reverse of reaction (1). However, the difference between H_2-TPR and CO-TPR activities is quite large for the same LSCF–GDC, which

Table 2
Total amount of CO formation during CO_2-TPO over Cu, Ag and Pt added L58SCF, LSCF, 100LSCF–50GDC[a] and GDC.

Materials	Amount of CO formation (mmol g^{-1})			
	L58SCF	LSCF	100LSCF–50GDC	GDC
Cu added	2.81	2.18	2.22	0.05
Ag added	2.79	2.03	2.10	0.09
Pt added	2.77	1.68	1.76	0.34
Without metal addition	2.76	1.64	1.75	0.01

[a] The number denotes the composition in weight.

Table 3
Total amounts of CO formation during CO_2-TPO, H_2 consumption during H_2-TPR and CO_2 formation during CO-TPR over various LSCF–GDC composites.

Materials	Amount of CO formation (mmol g^{-1})	Amount of H_2 consumption (mmol g^{-1})	Amount of CO_2 formation (mmol g^{-1})
LSCF	1.64	4.76	9.95
100LSCF–30GDC[a]	1.74	5.00	11.67
100LSCF–50GDC	1.75	5.08	11.84
100LSCF–70GDC	1.18	4.20	10.75
100LSCF–100GDC	1.11	4.16	8.99
GDC	0.01	2.40	2.98

[a] The number denotes the composition in weight.

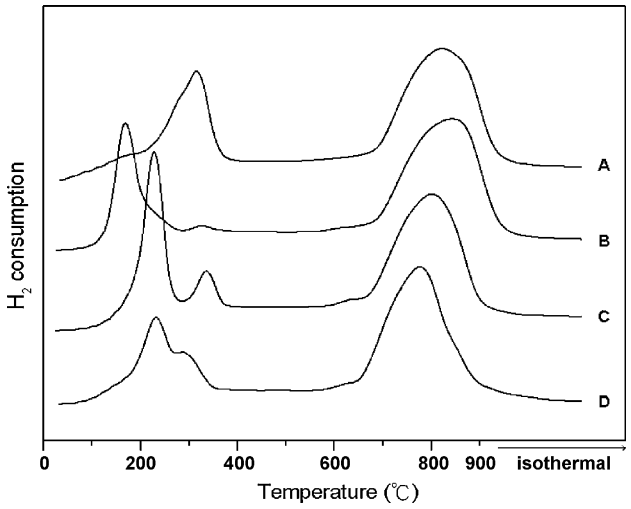

Fig. 5. H_2-TPR profiles: (A) Pt-LSCF, (B) Ag-LSCF, (C) Cu-LSCF, (D) LSCF.

should have the same property of oxygen transport during either H_2-TPR or CO-TPR; thus, the rate-determining step should be the surface catalytic reaction but not the process of oxygen transport from the lattice. Therefore, there is a similarity between the process of electrochemistry over SOFC anode and the process of chemistry in the H_2-TPR and CO-TPR analyses—that is, both have the surface catalytic reaction as the rate-determining step. Notably, also, the H_2-TPR and CO-TPR analyses are the well-known techniques for the characterization of oxidation activities of various catalysts; for the SOFC anode, the fuels include H_2 and CO, e.g., coal gas and synthesis gas, and thus both H_2 and CO oxidation activities have certain importance.

100LSCF–50GDC has the highest activity for either H_2 or CO oxidation among these LSCF–GDC composites and this activity is also higher than that of LSCF. This is the same as for the CO_2 reduction activity. Since the H_2 and CO oxidation activity of GDC is about one half and less than one-third of that of LSCF, respectively, the higher activity of 100LSCF–50GDC than LSCF should also be due to a synergistic effect of adding GDC into LSCF as for the CO_2 reduction activity. Again, adding too much GDC decreases the activity of the LSCF–GDC composite to become smaller than that of LSCF, as shown in Table 3.

Table 3 also shows that the activity of CO oxidation is dramatically higher than that of CO_2 reduction. Since CO_2 reduction can be a reverse reaction of CO oxidation, this dramatic difference indicates that the rate-determining step for CO oxidation is different from that for CO_2 reduction; the former is probably the adsorption step while the latter is the step of oxygen transport into the lattice of the materials; this will be clarified in Section 4.

3.4. H_2-TPR analysis for anode characterization

Fig. 5 shows the H_2-TPR profiles of LSCF and Pt, Ag and Cu added LSCF. The total amount of H_2 consumption during H_2-TPR over LSCF is presented in Table 3 and those over metal-added LSCF are presented in Table 4. These amounts show a trend Pt-LSCF > Cu-LSCF > Ag-LSCF > LSCF; thus, the effect of metal addition has a trend Pt > Cu > Ag. This trend for H_2 oxidation is different from that for CO_2 reduction, being Cu > Ag > Pt.

Fig. 6 shows that, for Cu-LSCF, the small peak at 350 °C before reduction disappears after a H_2-TPR run. This is associated with the disappearance of the segregated Cu species, which is due to the doping of the Cu species into the LSCF lattice; this will be clarified in Section 4.

Table 4
Total amounts of H_2 consumption during H_2-TPR and CO_2 formation during CO-TPR over Pt, Cu and Ag added LSCF and GDC.

Materials	Amount of H_2 consumption (mmol g^{-1})	Amount of CO_2 formation (mmol g^{-1})
Pt-LSCF	6.5	11.26
Cu-LSCF	5.72	10.9
Ag-LSCF	5.6	10.7
Pt-GDC	3.00	4.03
Cu-GDC	2.94	3.91
Ag-GDC	2.64	3.38

The SOFC anode is usually composed of GDC for SOFCs operating at intermediate temperatures, such as 800 °C [35]. Thus, GDC and Pt, Cu and Ag added GDC were studied in this work for comparison of the anodic activities. Fig. 7 shows H_2-TPR profiles of GDC and Pt, Cu and Ag added GDC. The total amount of H_2 consumption during H_2-TPR over GDC is presented in Table 3 and those over metal-added GDC are presented in Table 4. These amounts show a trend Pt-GDC > Cu-GDC > Ag-GDC > GDC; thus, the effect of metal addition also has a trend Pt > Cu > Ag. This indicates that adding Pt, Cu and

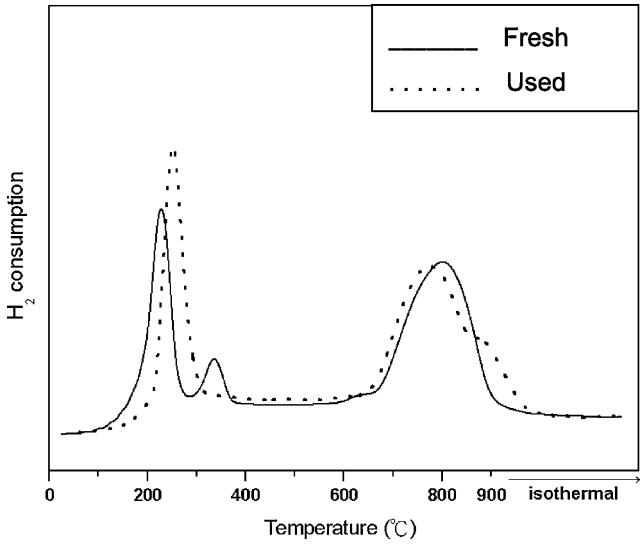

Fig. 6. H_2-TPR profiles of Cu-LSCF. The "used" sample is the one after an H_2-TPR run and then re-oxidized to perform the indicated test.

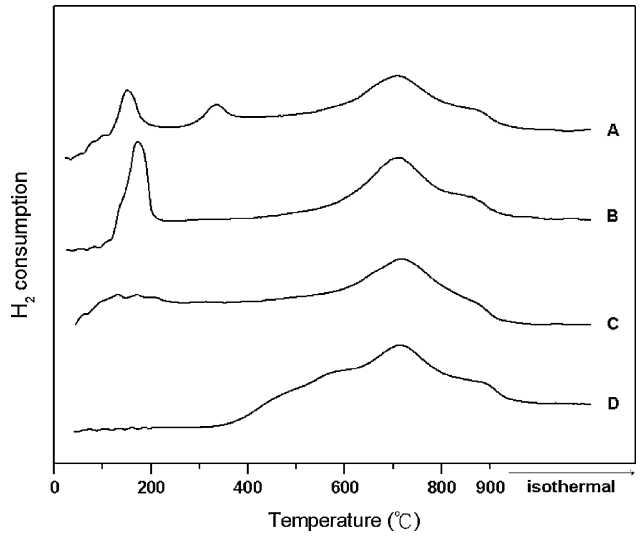

Fig. 7. H_2-TPR profiles: (A) Pt-GDC, (B) Cu-GDC, (C) Ag-GDC, (D) GDC.

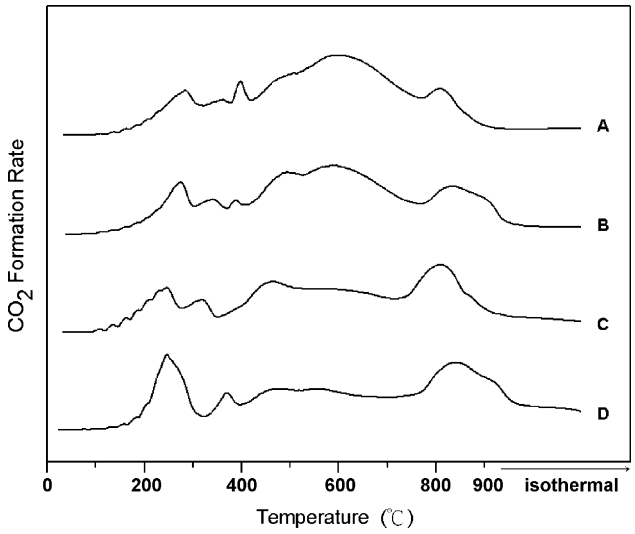

Fig. 8. CO-TPR profiles: (A) Pt-LSCF, (B) Ag-LSCF, (C) LSCF, (D) Cu-LSCF.

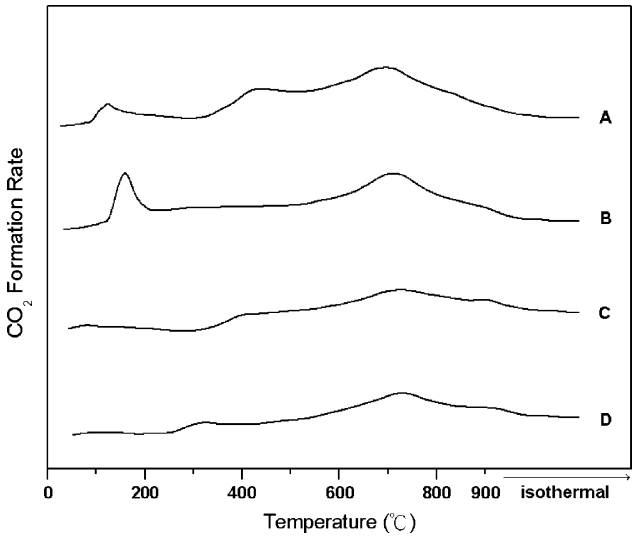

Fig. 9. CO-TPR profiles: (A) Pt-GDC, (B) Cu-GDC, (C) Ag-GDC, (D) GDC.

Ag to GDC has the same effect on the enhancement of H_2 oxidation activity as that of adding these metals to LSCF.

However, the H_2 oxidation activity of the LSCF series is about two times that of the GDC series. This is probably due to some metallic characteristics of LSCF; a comparison of the H_2-TPR profile of LSCF in Fig. 5 and that of GDC in Fig. 7 shows that LSCF has low temperature peaks at around 200–300 °C but GDC does not have these peaks, which are usually the characteristics of the metals.

3.5. CO-TPR analysis for anode characterization

Fig. 8 shows the CO-TPR profiles of LSCF and Pt, Ag and Cu added LSCF. There is almost continuous CO_2 formation after about 500 °C which is the temperature for CO disproportionation, which occurs via the Boudouard reaction [38]:

$$2CO \rightarrow CO_2 + C \quad (3)$$

The formation of residual carbon from the C species is confirmed by the amount of carbon removal after the CO-TPR test, as shown in Table 5. However, the C species formed via reaction (3) can be oxidized to form CO and/or CO_2 by the bulk lattice oxygen of GDC, which has a capability of self de-coking [39]:

$$C + O \rightarrow CO \quad (4)$$

$$C + 2O \rightarrow CO_2 \quad (5)$$

where O denotes the lattice oxygen of the oxygen–ion conducting materials such as LSCF and GDC. Thus, the amount of residual carbon, which is represented by carbon removal, is very much less than that of CO_2 formed via CO oxidation, as shown in Table 4.

Table 5
Carbon removal after CO-TPR, shown as the amount of CO_2 formation,[a] over Pt, Ag and Cu added LSCF and GDC.

Materials	Amount of CO_2 formation (mmol g^{-1})
Pt-LSCF	0.69
Ag-LSCF	0.45
LSCF	0.23
Cu-LSCF	0.14
Pt-GDC	0.09
Ag-GDC	0.08
GDC	0.05
Cu-GDC	0.01

[a] Only CO_2 but no CO was detected during this carbon removal process.

Additionally, the CO-TPR activities show a trend Pt-LSCF > Cu-LSCF > Ag-LSCF > LSCF; thus, the effect of metal addition has a trend Pt > Cu > Ag. This trend for CO oxidation is the same as that for H_2 oxidation.

Fig. 9 shows the CO-TPR profiles of GDC and Pt, Cu and Ag added GDC. The total amount of CO_2 formation during CO-TPR over GDC is presented in Table 3 and those over metal-added GDC are presented in Table 4. These amounts also show a trend Pt-GDC > Cu-GDC > Ag-GDC > GDC and a metal-addition effect Pt > Cu > Ag. Therefore, adding Pt, Cu and Ag to GDC has the same effect on the enhancement of CO oxidation activity as that of adding these metals to LSCF.

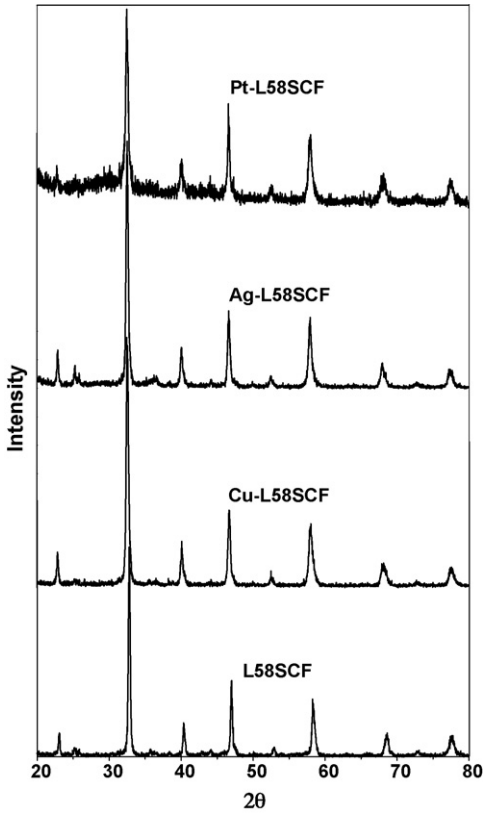

Fig. 10. XRD spectra of L58SCF and Cu, Ag and Pt added L58SCF.

However, the CO oxidation activity of the LSCF series is about three times that of the GDC series. This is also due to the metallic characteristics of LSCF; a comparison of the CO-TPR profile of LSCF in Fig. 8 and that of GDC in Fig. 9 shows that LSCF has a low temperature peak at around 200–300 °C but GDC does not have this peak, which is usually the characteristic of the metal.

Table 4 shows that the effects of metal addition on the enhancement of both H_2 and CO oxidation activities have the same trend Pt > Cu > Ag. However, for traditional alumina-supported catalysts, Pt addition is well known to result in a higher CO oxidation activity than Cu addition [40]. Section 4 will state the reason for this difference. Additionally, Table 4 shows that the activities of CO oxidation are higher than those of H_2 oxidation; this is the same as that over the LSCF–GDC composites. The LSCF series have higher H_2 oxidation activities and much higher CO oxidation activities than the GDC series; thus, pure LSCF can be a better SOFC anode material than pure GDC, especially when H_2 and CO are used as the fuel. Notably, GDC is generally mixed with Ni to form a cermet but not used alone for the SOFC anode.

Although Cu-LSCF has a better CO oxidation activity than those of Ag-LSCF and LSCF, the amount of residual carbon over Cu-LSCF after CO-TPR is less than those over Ag-LSCF and LSCF, as shown in Table 5; this is the same over the GDC series. This behavior is associated with a higher de-coking capability of Cu-LSCF than those of Ag-LSCF and LSCF; this will be clarified in Section 4. However, Table 5 also shows that the amounts of residual carbon over the GDC series are much smaller than those over the LSCF series; this is attributed to the much smaller CO-TPR activities of the GDC series than those of the LSCF series, which should be associated with much smaller activities of CO disproportionation.

4. Discussion

The effect of adding Cu, Ag and Pt to LSCF for the cathodic reduction activity has been shown to follow a trend Cu > Ag > Pt. This can be explained by the oxygen affinities of the metals, which have a trend Cu > Ag > Pt, corresponding to the oxidizing property of these metals. A higher oxygen affinity means that the metal can be oxidized more easily; restated, the metal can take in more oxygen from the gas phase or other source, the latter being the lattice oxygen of LSCF or GDC in this work, and thus its oxidation rate can be higher. If the amount of the oxygen species taken in by the metal is more than that can be transported away or consumed, the metal is oxidized to metal oxide and thus its metallic activity is lost. In this case, if the oxygen affinity of the metal is higher, its extent of being oxidized is higher and thus its extent of the activity loss is higher; thus, higher oxygen affinity leads to lower activity. This may explain the trend Cu < Ag < Pt for the CO_2-TPO activities of the GDC series, as shown in Table 2. Notably, the O species produced by CO_2 dissociation can oxidize the metals.

However, if the oxygen species taken in by the metal can be transported away or consumed quickly so that these oxygen species would not stay on the metal surface, higher rate of oxygen-taken-in can mean higher activity of the materials. The ability of transporting the oxygen species away is associated with the oxygen reduction activity of metal-added LSCF as the SOFC cathode. High oxygen reduction activity means that the rate of oxygen transport from the metal surface into the oxygen vacancy in the LSCF lattice is fast; this oxygen-transport rate can be enhanced by doping the metal into the LSCF lattice, which should increase the metal–lattice interaction. Higher oxygen affinity results in higher rate of oxygen-taken-in; if the oxygen species can be transported away faster than taken in, the oxygen reduction process becomes faster. Therefore, higher oxygen affinity can lead to higher activity of oxygen or CO_2 reduction. For this case, the rate-determining step for oxygen or CO_2 reduction is oxygen transport into the lattice of the materials.

Carter et al. [41] pointed out that doping metal into the ABO_3 structure of the perovskites may increase the rate of oxygen transport. The doping of the Cu species into the ABO_3 structure, the lattice, of LSCF may be confirmed by the disappearance of the segregated Cu species after 900 °C treatment, as shown in Fig. 6. This Cu doping ability comes from that the cation radius of Cu^{2+} (0.73 Å) [42] is close to that of B-site Co^{2+} (0.75 Å) [43]. The capability of Cu doping into the LSCF B-site has been shown by the formation of $(La,Sr)(Co,Cu)O_3$ [18]. However, the impregnated Cu cation may not be able to be fully doped into the LSCF B-site after the LSCF material has been calcined; partial doping may be more possible, which can still lead to a close interaction of Cu with the LSCF lattice. Therefore, the rate of oxygen transport from Cu metal to the LSCF lattice can be increased.

The doping of the Cu, Ag and Pt species into the ABO_3 structure of LSCF may be confirmed by the X-ray diffraction (XRD) spectra shown in Fig. 10. A systematical shift of the diffraction angles of the XRD peaks to lower ones occurs for metal-added LSCF. Dow and Huang [44] reported that, after reduction at 800 °C, the 1 wt.% Cu added YSZ composite shows penetration of copper atoms into the YSZ bulk, which has been ascertained by a systematical shift of the diffraction angles of the XRD peaks to lower ones; additionally, this shift still occurs after re-oxidation. Notably, the calcinations of metal-added LSCF were carried out at 800 °C in this work. Therefore, the Cu, Ag and Pt species have been doped, at least partially, into the LSCF lattice.

The ability of consuming the oxygen species is associated with the self de-coking capability of metal-added GDC or LSCF during CO-TPR. High capability of self de-coking means that the produced C species over the metal is quickly oxidized by the O species taken in by the metal, with the O species coming from the lattice of LSCF or GDC in this work. Therefore, higher oxygen affinity, which results in higher rate of oxygen-taken-in, leads to higher capability of self de-coking. Notably, both the O species from oxygen or CO_2 reduction and the C specie for self de-coking are reaction intermediates and have to be removed so that the reaction process can be completed; thus, the oxygen affinity can play a determining role as discussed in the above. However, for either H_2 or CO oxidation, the rate-determining factor can be the activity of H_2 or CO adsorption but not the oxygen affinity.

5. Conclusions

(1) The temperature-programmed techniques can be used for the characterization of the cathode or the anode materials and allow an easy screening of the materials as the SOFC electrodes.
(2) The effects of Cu, Ag and Pt addition to LSCF for the cathodic reduction activity and the anodic oxidation activity are different, that is, Cu > Ag > Pt for reduction and Pt > Cu > Ag for oxidation.
(3) The CO oxidation activities are higher or much higher than the H_2 oxidation activities for either LSCF or GDC series.
(4) Adding GDC to LSCF can increase both reduction and oxidation activities.
(5) The LSCF–GDC composite has a maximum activity for either reduction or oxidation when LSCF/GDC is 2 in weight.

References

[1] F. Tietz, V.A.C. Haanappel, A. Mai, J. Mertens, D. Stover, J. Power Sources 156 (2006) 20.
[2] V.A.C. Haanappel, A. Mai, J. Mertens, Solid State Ionics 177 (2006) 2033.
[3] W.H. Kim, H.S. Song, J. Moon, H.W. Lee, Solid State Ionics 177 (2006) 3211.
[4] Z. Lei, Q. Zhu, L. Zhao, J. Power Sources 161 (2006) 1169.
[5] J. Liu, A.C. Co, S. Paulson, V.I. Birss, Solid State Ionics 177 (2006) 377.

[6] F. Qiang, K. Sun, N. Zhang, X. Zhu, S. Le, D. Zhou, J. Power Sources 168 (2007) 338.
[7] H. Uchida, S. Arisaka, M. Watanabe, Solid State Ionics 135 (2000) 347.
[8] K. Sasaki, J. Tamura, H. Hosoda, T.N. Lan, K. Yasumoto, M. Dokiya, Solid State Ionics 148 (2002) 551.
[9] V.A.C. Haanappel, D. Rutenbeck, A. Mai, S. Uhlenbruck, D. Sebold, H. Wesemeyer, B. Röwekamp, C. Tropartz, F. Tietz, J. Power Sources 130 (2004) 119.
[10] H.J. Hwang, J.W. Moon, S. Lee, E.A. Lee, J. Power Sources 145 (2005) 243.
[11] F. Liang, J. Chen, J. Cheng, S.P. Jiang, T. He, J. Pu, J. Li, Electrochem. Comm. 10 (2008) 42.
[12] S. Wang, T. Kato, S. Nagata, T. Honda, T. Kaneko, N. Iwashita, M. Dokiya, Solid State Ionics 146 (2002) 203.
[13] J. Zhang, Y. Ji, H. Gao, T. He, J. Liu, J. Alloys Compounds 395 (2005) 322.
[14] S.P. Simner, M.D. Anderson, J.E. Coleman, J.W. Stevenson, J. Power Sources 161 (2006) 115.
[15] C.L. Chang, T.C. Lee, T.J. Huang, J. Appl. Electrochem. 26 (1996) 311.
[16] C.L. Chang, C.C. Hsu, T.J. Huang, J. Solid State Electrochem. 7 (2003) 125.
[17] C.L. Chang, T.C. Lee, T.J. Huang, J. Solid State Electrochem. 2 (1998) 291.
[18] K. Yasumoto, Y. Inagaki, M. Shiono, M. Dokiya, Solid State Ionics 148 (2002) 545.
[19] H.C. Yu, K.Z. Fung, J. Power Sources 133 (2004) 162.
[20] A. Hartley, M. Sahibzada, M. Weston, I.S. Metcalfe, D. Mantzavinos, Catal. Today 55 (2000) 197.
[21] Y.H. Huang, R.I. Dass, Z.L. Xing, J.B. Goodenough, Science 312 (2006) 254.
[22] X.J. Chen, Q.L. Liu, S.H. Chan, N.P. Brandon, K.A. Khor, Electrochem. Comm. 9 (2007) 767.
[23] A.A. Yaremchenko, A.A. Valente, V.V. Kharton, I.A. Bashmakov, J. Rocha, F.M.B. Marques, Catal. Comm. 4 (2003) 477.
[24] A. Hornés, D. Gamarra, G. Munuera, J.C. Conesa, A. Martínez-Arias, J. Power Sources 169 (2007) 9.
[25] J.B. Wang, J.C. Jang, T.J. Huang, J. Power Sources 122 (2003) 122.
[26] W.Z. Zhu, S.C. Deevi, Mater. Sci. Eng. A 362 (2003) 228.
[27] W.G. Wang, M. Mogensen, Solid State Ionics 176 (2005) 457.
[28] E.P. Murray, M.J. Sever, S.A. Barnett, Solid State Ionics 148 (2002) 27.
[29] A. Sin, E. Kopnin, Y. Dubitsky, A. Zaopo, A.S. Aricò, L.R. Gullo, D. La Rosa, V. Antonucci, J. Power Sources 145 (2005) 68.
[30] F.S. Baumann, J. Fleig, H.U. Habermeier, J. Maier, Solid State Ionics 177 (2006) 1071.
[31] T.J. Huang, S.Y. Jhao, Appl. Catal. A 302 (2006) 325.
[32] T.J. Huang, T.C. Yu, Catal. Lett. 102 (2005) 175.
[33] T.J. Huang, H.J. Lin, T.C. Yu, Catal. Lett. 105 (2005) 239.
[34] T.J. Huang, C.H. Wang, J. Power Sources 163 (2006) 309.
[35] T.J. Huang, M.C. Huang, Chem. Eng. J. 135 (2008) 216.
[36] T.J. Huang, J.F. Li, J. Power Sources 181 (2008) 62.
[37] A. Mai, V.A.C. Haanappel, S. Uhlenbruck, F. Tietz, D. Stover, Solid State Ionics 176 (2005) 1341.
[38] A. Govindaraj, R. Sen, A.K. Santra, B.V. Nagaraju, Mater. Res. Bull. 33 (1998) 663.
[39] T.J. Huang, C.H. Wang, Chem. Eng. J. 132 (2007) 97.
[40] T.J. Huang, H.D. Hwu, J. Chin. Inst. Chem. Eng. 17 (1986) 69.
[41] S. Carter, A. Selcuk, R.J. Chater, J. Kajda, J.A. Kilner, B.C.H. Steele, Solid State Ionics 53–56 (1992) 597.
[42] Q.R. Feng, J.D. Guo, X.L. Xu, I. Zhang, X. Zhu, S.Q. Feng, Solid State Comm. 94 (1995) 21.
[43] R.W. Grimes, S.P. Chen, J. Phys. Chem. Solids 61 (2000) 1263.
[44] W.P. Dow, T.J. Huang, J. Catal. 147 (1994) 322.